Experimental evaluation of a commercial scale dew-point cooler with different air distribution configurations

Muhammad Usama[a,b,c,*], Aashir Iqbal[b,c], Tahmid Hasan Rupam[a], Bidyut Baran Saha[d,e]

[a] *University of Texas at Austin, 2515 Speedway, Austin, TX 78712, United States*
[b] *Bfreeze Pvt Ltd, Ghouri Town Phase-5. Rawalpindi, Pakistan*
[c] *National University of Science and Technology (NUST), H-12, Islamabad, Pakistan*
[d] *International Institute for Carbon-Neutral Energy Research, Kyushu University, 744 Motooka, Nishi-ku, Fukuoka 819-0395, Japan*
[e] *Mechanical Engineering Department, Kyushu University, 744 Motooka, Nishi-ku, Fukuoka 819-0395, Japan*

Abstract

Dew-point evaporative coolers based on the Maisotsenko cycle (M-cycle) offer significantly higher energy efficiency than conventional vapor-compression cooling systems while avoiding refrigerant emissions. However, their performance depends on airflow configuration, working air ratio, and the recirculation strategy used to generate evaporative cooling. In this study, a commercial-scale cross-flow M-cycle indirect evaporative cooler with a maximum cooling capacity of 12.2 kW (3.5 tons) was experimentally evaluated under different airflow and recirculation configurations. The system incorporated two controllable recirculation stages that allowed independent adjustment of the working air ratio, r, and a newly defined working air distribution ratio, r_d, representing the distribution of recirculated air drawn from upstream and downstream sections of the dry channel. Experiments were conducted across a wide airflow range (100-11,000 m^3/hr) and varying inlet humidity conditions while maintaining constant inlet temperature. The results show that increasing the working air ratio enhances the temperature drop and dew-point effectiveness but reduces the coefficient of performance (COP) due to increased fan power consumption and pressure losses. An optimal working air ratio of $r = 0.33$ was identified for maximizing cooling capacity and COP. The study further demonstrates that preferentially drawing equivalent volumes of recirculated air from downstream and upstream of the dry channel significantly improves performance. The optimal working air distribution ratio was found to be $1.1 \leq r_d \leq 1.3$, yielding the lowest product air temperature and highest COP. These findings highlight the importance of airflow distribution design in M-cycle heat exchangers and provide guidance for optimizing recirculation strategies in large-scale dew-point cooling systems.

Keywords: chiller; dewpoint; evaporative cooling; HVAC; M-cycle

*Corresponding author: Muhammad Usama. Email: usama_cto@bfreeze.com
**Corresponding author: Bidyut Baran Saha. Email: saha.baran.bidyut.213@m.kyushu-u.ac.jp

1. Introduction

As the average global temperatures rise, so does the energy load on Air-Conditioning and cooling systems [1]. This has caused a growing need for more energy-efficient cooling solutions to manage the power load on the grid and control the Carbon emissions associated with Air-Conditioning [2, 3], mitigating Carbon emissions to aid the efforts to . There have been significant advancements in improving the energy efficiency of vapor-compression systems, such as reducing condenser temperatures [4, 5], recovering waste heat from compressors [6], incorporating multi-stage evaporation and condensation [7], and using an ejector to enhance the vapor uptake from the evaporator [8]. Several improvements have also been made in evaporative cooling systems. Energy efficiency for evaporative systems is much higher than that for Vapor Compression systems [9], and, due to the lack of high Global Warming Potential (GWP) refrigerants, CO2 emissions from chemical leakage are also non-existent [10]. But the increase in Relative Humidity (RH) due to evaporation is a major bottleneck limiting the environmental comfort provided by evaporative Air Conditioning systems [11, 12].

The improvements in evaporative cooling systems are related to achieving low temperatures without significantly increasing the Relative Humidity (RH). To achieve this, Indirect Evaporative Coolers (IDECs) have gained traction as opposed to Direct Evaporative Coolers (DECs) as illustrated in Fig # 1 (a) and Fig # 1 (b) respectively [13, 14]. Indirect evaporation achieves low temperatures via evaporative cooling but without allowing humid air into the space that is being air-conditioned, keeping its RH low [14, 15].

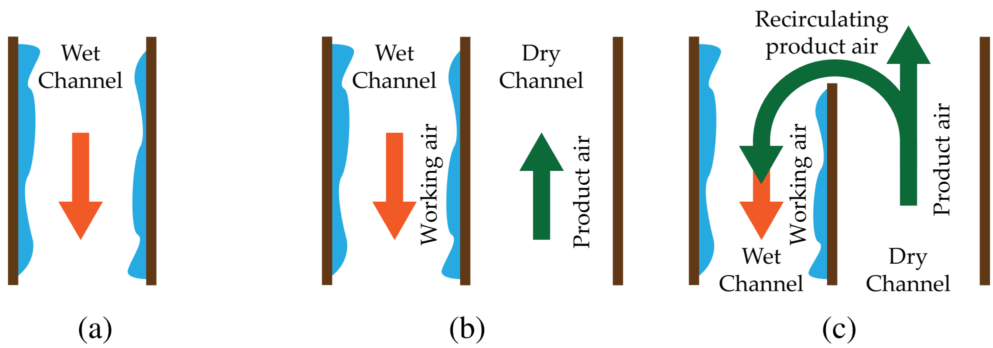

Figure 1: Illustrations of (a) Direct evaporative cooling, (b) Indirect evaporative cooling, (c) Indirect evaporative cooling with dry air recirculation.

The Maisotsenko cycle (M-cycle) is a type of IDEC that uses multiple passes of indirect cooling of air to attain a product air temperature that is much lower than the Wet Bulb Temperature (WBT) and ideally close to the Dew Point Temperature (DPT) [14, 16]. This is achieved by using a part of the indirectly cooled product air to conduct evaporation. The exergy or cooling potential created by the subsequent cycles of indirect evaporation continues to drop the product air temperature as briefly illustrated in Fig # 1 (c) [17, 18]. The temperature drop in an IDEC based on the M-cycle reduces with each subsequent indirect cooling pass, meaning that the highest temperature drop is achieved as the product air drops from Dry Bulb Temperature (DBT) to WBT, followed by its drop from WBT to a temperature between DPT and WBT in the first M-cycle pass, and so on [18, 19]. Fig # 2 shows these incremental temperature drops [18, 19]. Fig # 2 further illustrates the thermodynamic principle behind the M-cycle shown schematically in Fig # 1 (c). While Fig # 1 (c) demonstrates the physical recirculation of cooled product air into the wet channel, Fig # 2 explains the corresponding psychrometric temperature changes occurring during each recirculation stage.

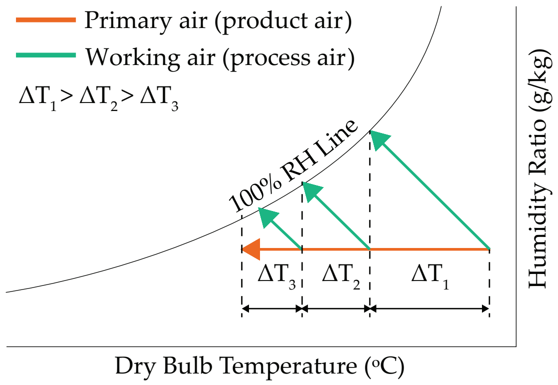

Figure 2: A psychrometric chart showing incremental temperature drops as primary air is sequentially mixed with working air.

Recent research on the M-cycle has focused on optimizing parameters such as flow rate, cooling capacity, humidity, COP, and dew-point effectiveness across different configurations. Duan et al [20] designed and experimentally tested a counter-flow REC with vertical channels, reporting wet-bulb effectiveness values of 0.747-0.820 and energy savings of 13-58% across various Chinese climate zones. Ma et al [21] developed and real-life tested a 100 kW vertical-channel dew-point cooling system in a live data centre, achieving an average COP of 29.7 and up to 90% energy savings compared to conventional vapor compression systems. Jradi and Riffat [22] experimentally and numerically evaluated a cross-flow dew-point cooler with vertical channels, reporting a wet-bulb effectiveness of 112% and dew-point effectiveness of 78% at a working-to-intake air ratio of 0.33. Weragoda et al [23] numerically assessed capillary-driven evaporative coolers with vertically aligned porous media, finding that wick porosity is the most significant factor influencing dry-out height and saturation. Wang et al [24], Liu et al [25], and Khalid et al [26] developed cross-flow and counter-flow dew-point evaporator configurations using vertical channels. Huang et al [27] compared vertically and horizontally aligned channels for indirect evaporative cooling and found that IDECs made with vertically aligned channels demonstrated lower specific energy consumption. Xu et al [28] had the same finding and explained that the gravity assisted water supply in the wet channel leads to better distribution of water for evaporation.

The airflow configuration through the wet and dry channels also plays a role in the performance of the dew-point cooler. The channels can flow in parallel-flow, cross-flow, or counter-flow configurations [19, 29]. Wang et al [24] developed an M-cycle IDEC with a counter-flow configuration, and found that COP increases proportionally with air flow rate. However, it was found to be at its maximum at a working ratio of 0.5, defined as the ratio of the working air in the wet channel to the total inlet air [30, 29]. Lin et al. [31] also developed a cross-flow dew-point cooler with a similar geometry and found that the COP drops with the cooling capacity and the dew point effectiveness of the chiller.

Although recent studies have extensively investigated M-cycle configurations, flow rates, and working air ratios, the distribution of recirculated air across different stages of the dry channel has received little attention. Experimental investigations into this parameter are even scarcer. The working ratios in large capacity M-cycle chillers are too high, meaning that a significant proportion of the product air is typically lost to attain a high dew point effectiveness [31, 12]. This comes at the cost of a drop in COP [15, 32]. Moreover, the coatings used on the wet channel are typically either not conductive enough or not hydrophilic enough [17, 33]. While material conductivity and wettability of wet channel surfaces present their own tradeoffs, the more critical and underexplored challenge lies in optimizing the working air ratio and its distribution across recirculation stages.

This study is aimed at mitigating the aforementioned tradeoffs. An IDEC based on the M-cycle cross-flow was designed, manufactured, and tested for its performance. This was a large-scale unit with a maximum cooling capacity of 12.2 kW or 3.5 Tons. Two recirculation passes were employed with a controllable flow rate for recirculating air to allow for optimization between energy efficiency and overall temperature drop. Instead of using holes in the interface between dry and wet channels for recirculation, offshoot ducts were created to minimize pressure losses and thus the pumping power needed to circulate air. Perforated plates can be used to recirculate air as shown in Fig # 3 (a)[30]. But there is no categorical advantage to using perforations as opposed to forced or ducted recirculation [34]. Fig # 3 (b) shows the ducts located at different spots in the heat exchanger to recirculate air, forming the recirculation with cross-flow configuration used in this study. This is a multi-stage M-cycle configuration since different fractions of the product air can be recirculated to mix with the working air [12].

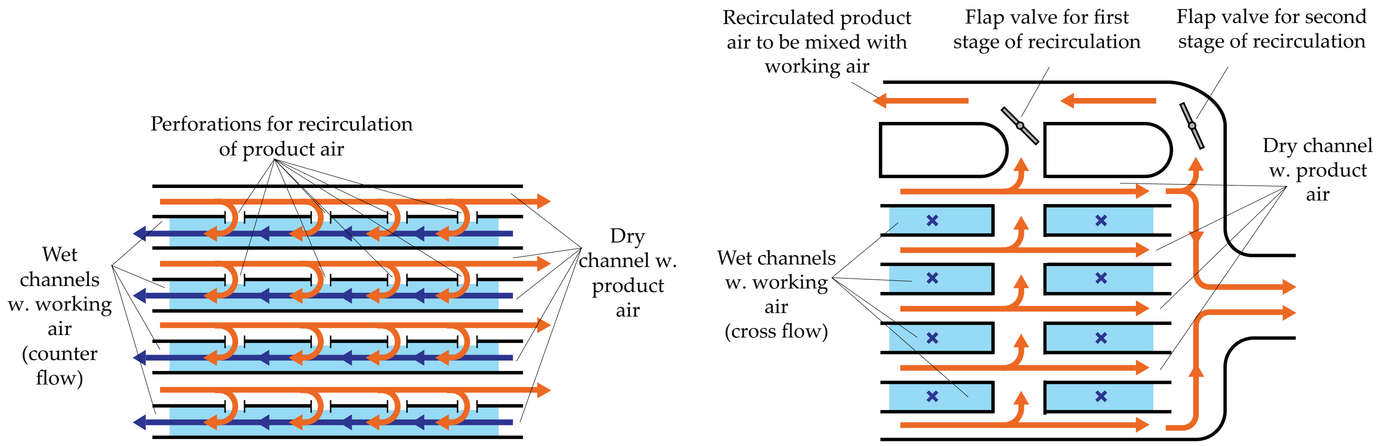

(a) (b)

Figure 3: Recirculation of product air via (a) perforations in the channels, (b) ducts in the channels.

As Fig # 3 (b) shows, the unit developed for this study allows us to adjust the flow rate of the recirculating air from different locations (50% of the way and 100% of the way through the dry channel). Using this design feature, the optimal location to draw product air from the dry channel to mix it with the working air was also evaluated.

2. Materials and Methodology

This section describes the design and construction of the experimental setup, the instrumentation, and the data collection methods.

2.1. Materials, design, and construction

The interface was created using Aluminum 5052 foils (2.5% Mg, 0.25% Cr) to provide high conductivity and corrosion resistance when used with tap water (TDS $\leq$ 200). A 5x6x5 ft (LxWxH) crossflow M-Cycle heat and mass exchanger was designed as depicted in Fig # 4 (a). This heat and mass exchanger was connected to a water and air distribution system, all packaged into a casing as shown in Fig # 4 (b).

(a) (b) (c)

Figure 4: (a) Manufactured heat and mass exchanger, (b) Packaged Dew-point cooler using the heat and mass exchanger, (c) illustration of laid up sheets allowing cross flow of wet and dry channels.

1.5 mm thick Aluminum sheets were laid up and separated by 0.25" thick rubber panels, laid 2" apart to keep the structure standing. These rubber pannels were pasted on the Aluminum sheets in alternating orientations to form a cross-flow configuration as shown in Fig # 4 (c).

Each air/water intake channel (dry and wet channel) was thus 30x2x0.25" (LxWxH). A cross-section of the heat and mass exchanger is illustrated in Fig # 4 (a). Two ducts with mechanically controlled flap valves were installed in the middle and the end of the heat exchanger to draw the desired flow rate of dry and cooled product air as illustrated in Fig #3 (b). This product air was recirculated and mixed with the working air flowing perpendicular to the dry channels due to the cross-flow configuration of the heat and mass exchanger. Finally, this culminated in a packaged IDEC unit as shown in Fig # 4 (c).

A Yubinchuang SLG40-100 750 W centrifugal pump was used to circulate water from the bottom of a 1.2 ft chamber at the bottom of the IDEC unit to circulate water through the wet channel. The pump inlet was placed such that there was a 0.97 ft water head. The water flow rate was measured using an IP6X mass flow meter attached in series with the piping. Two identical Global Industrial™ B703062 2250 W centrifugal blowers were used to pump air through the heat and mass exchanger, one for the dry channel and the other for the wet channel. Further specifications of the rotary equipment is listed in Talbe # 1.

Table 1: Equipment specifications.

Equipment	**Manufacturer**	**Model**	**Specifications**	**Dimensions (WxHxD)**
Digital micrometer	Fowler	Xtra-Value II	Res: 0.001mm, Acc:$\pm$0.004mm	9.0"x4.0"x1.5"
Vernier caliper	Sangabery	S-0802	Max: 6 in, LC: 0.1 mm	9.4"x3.1"x0.6"
Centrifugal fan	Global Industrial™	HADP14	3 HP, 1 PH, TEFC, 1575 CFM	8" inlet, 6" outlet
Centrifugal pump	SucceBuy	ZXQ1000-B	700 W, 4148 GPH, 10 m	6.42"x6.1"x12.52"
Power Analyzer	Fluke Corporation	434-II	1-1000 V, 5-6000 A, 0-6 kW	10.1"× 6.7"×2.5"
Anemometer	Metravi instruments	AVM-10	Acc: $\pm$ 5 m/s, Rng: 0.1-25 m/s	6.14"x2.64"x1.1"
Hygrometer	Fisher Scientific	1166120	Acc:$\pm$ 2.5, Rng:-10-95% RH	1"x2.5"x10.5"
TDS meter	Apera Instruments	SX723	Acc: ±1% F.S, Rng: 0-200 mS/cm	2.6"×4.7"×1.2"
Pressure transducer	AUTEX	100psi SS	Acc: ±1% F.S, Rng: 0-100 Psi	5.91"×3.94×0.98"
Thermocouple	Proster	Type K	Acc: 1.5%, Rng: -50-300°C	5.71"×0.01"×0.01"
Weighing scale	Scientific Industries Inc.	AD60	Max: 60g, Res: $\pm$ 0.001g	9.4"x10.7"x3.6"

2.2. Instrumentation, control, and data collection

The process and product air's speeds were measured using a Metravi AVM-10 anemometer, and as the air exited through a 4.5x4.75 ft (LxW) window, the air speed was converted to air volume flow rate using the wetted surface areas of the dry and wet channel outlet ducts.

The air temperature and humidity were measured using an EGT K-type thermocouple and an SHT20 hygrometer, respectively. Pressure transducers and thermocouples were installed at the beginning, 25%, 50%, 75%, and 100% of the way in both the dry and wet channels to measure the pressure and temperature drop. However, these instruments were only added in one wet channel and one dry channel each.

The water pump was controlled to deliver a constant flow rate to the wet channels using a rheostat. The airspeed of the fan was controlled with the feedback from the anemometer to maintain a constant air flow rate. The air drawn from each of the two stages of recirculation, as shown in Fig # 3 (b) to maintain r_d, was evaluated using the pressure differential across each stage of recirculation.

The inlet air humidity was varied while maintaining the same inlet air temperature using a 3 kW resistive heater, a water evaporator, and a Silica gel mesh placed at the inlet of the dew point cooler. To reduce the humidity below ambient conditions while retaining ambient temperature, the inlet air was dried with Silica gel. But to increase the humidity above ambient conditions, a water evaporator was used to add humidity, and the humidified and cooled air was heated with a resistive heater to reach ambient temperature. The power of the resistive heater was PID controlled against temperature and humidity feedback, maintaining inlet temperature to $\pm 1.5\%$ and the inlet humidity to within $\pm 2.4\%$ of the target value and .

The water quality in terms of its salinity was measured using an SX723 TDS meter by Apera Instruments, which was calibrated against known electrical conductivities of NaCl solution. The rise in TDS as water evaporated from the wet channel and the remaining water became more concentrated in salts was continuously monitored. Water circulating through the wet channels was discarded when the TDS level crossed 5000 ppm and replaced with fresh tap water. The fresh water was not treated prior to use to limit the water treatment cost [35], but the quality of the incoming water was monitored prior to uptake to ensure that the TDS level did not make the material susceptible to scaling damage. This was done to ensure the health of the dew-point cooler and prevent scaling of the walls in the wet channel.

2.3. *Performance evaluation*

Using the cooling system explained in section # 2.1 and instrumentation explained in section # 2.2, several performance indicators were evaluated. The mass flow rates of the product and working air were measured with an anemometer. The air speed was multiplied by the cumulative cross-sectional area of the channels to find the volumetric flow rate through the channels. The volumetric flow rate was, in turn, multiplied by the air density to find out the mass flow rate of the air [36].

$$\dot{V} = \vec{v} \times A_c \tag{1}$$

$$\dot{m} = \rho \times \dot{V} \tag{2}$$

The total temperature drop in the product air is defined as the range of a cooling system and is evaluated using the inlet and outlet temperatures for the product air flowing through dry channels [37],

$$\Delta T_{range} = T_{p,i} - T_{p,f} \tag{3}$$

The cooling capacity is defined as the total amount of heat load that the cooling system can remove. It is evaluated using ΔT_{range} and the airflow rate through the dry channels.

$$\dot{Q}_c = \dot{m} \times C_p \times \Delta T_{range} \tag{4}$$

The Coefficient of Performance (COP) is defined as the ratio between the heat power that is removed by a cooling system $\dot{Q}_c$ to the electrical or thermal power consumed $\dot{Q}_{e,in}$. [18].

$$COP = \frac{\dot{Q}_c}{\dot{Q}_{e,in}} \tag{5}$$

The Energy Efficiency Ratio (EER) is the cooling output in BTU/hr per Watt of input power [18, 38, 39].

$$EER = COP \times 3.41 \tag{6}$$

The Wet Bulb Effectiveness (η_{WB}) and Dew-point Effectiveness (η_{DP}) are measured by how closely the final product air temperature $T_{p,f}$ approaches the Wet Bulb Temperature T_{WB} and the Dew-point temperature T_{DP} [37, 12].

$$\eta_{WB} = \frac{\Delta T_{range}}{\Delta T_{WB}} = \frac{T_{p,i} - T_{p,f}}{T_{p,i} - T_{WB}} \tag{7}$$

$$\eta_{DP} = \frac{\Delta T_{range}}{\Delta T_{DP}} = \frac{T_{p,i} - T_{p,f}}{T_{p,i} - T_{DP}} \tag{8}$$

The product air ratio, or intake air ratio, is defined as the ratio of the final product air to the total incoming air in the dry channels. In an IDEC without any recirculation of product as depicted in Fig # 1 (b), the product air ratio would be 1.0 since none of it would be lost for recirculation. But a product air ratio from 0.3-0.9 is typically reported in literature and industrial practice, meaning that 10-70% of the product air can be sacrificed to be mixed with the working air to achieve temperatures lower than WBT [12, 18, 40, 41]. The product air ratio is defined as,

$$r = \frac{\dot{V}_{p,f}}{\dot{V}_{in}} \tag{9}$$

The overall recirculating air is the sum of the air being recirculated from Valve 1 and Valve 2.

$$\dot{V}_{p,f} = \dot{V}_1 + \dot{V}_2 \tag{10}$$

Since the design used in this study allows for controlling the fraction of product air drawn from the dry channel at different locations by controlling the dry air flowing from Valve 1 and Valve 2, one new parameter was introduced to study the impact of where most of the recirculating dry air was coming from. This parameter is called the working air distribution ratio or r_d.

$$r_d = \frac{\dot{V}_2}{\dot{V}_1} \tag{11}$$

Controlling the flowrates from upstream V_1 and downstream V_2 locations allows for the investigation of optimal locations where dry air should be drawn to improve ΔT_{range}, $\dot{Q}_c$, COP, EER, η_{WB}, and η_{DP}. Fig # 5 shows different valve configurations to control upstream and downstream flow rates V_1 and V_2 to create different dry air ratios r_d.

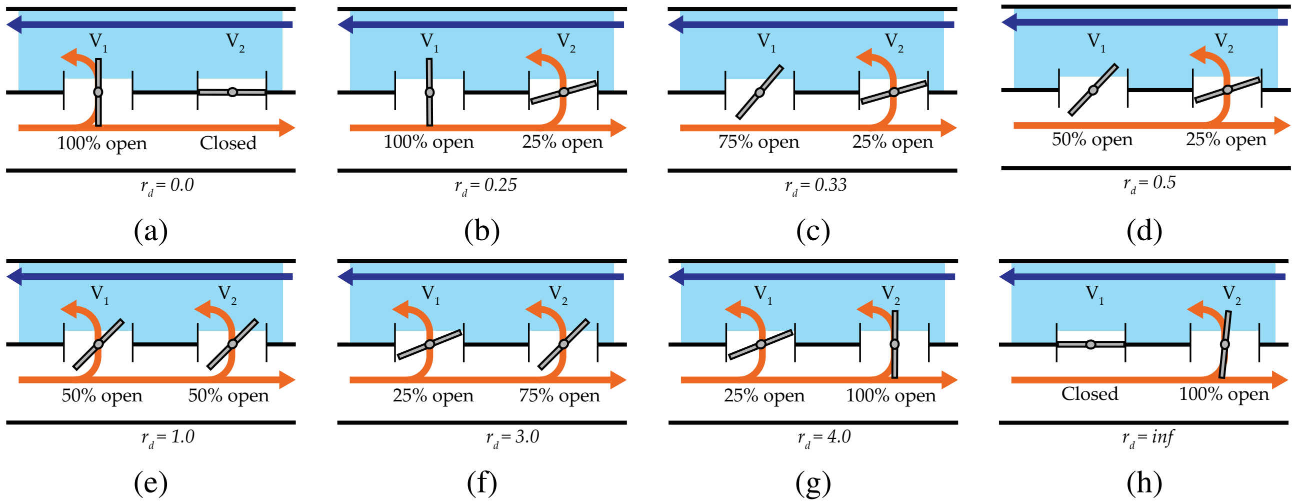

Figure 5: Illustration of different flow distribution ratios r_d tested (a) $r_d = 0.0$, (b) $r_d = 0.25$, (c) $r_d = 0.33$, (d) $r_d = 0.50$, (e) $r_d = 1.0$, (f) $r_d = 3.0$, (g) $r_d = 4.0$, (h) $r_d = \infty$.

2.4. Uncertainty analysis

The uncertainty in each parameter was based on taking multiple readings under similar conditions over a short time interval to maintain consistent environmental conditions. The maximum uncertainty values listed in Table # 2 are based on five (5) repeated measurements. Using twice the standard deviation, a 95% confidence interval for the uncertainty band was selected [42, 43]. For the parameters that were evaluated using the readings from other parameters, such as COP, dew point efficiency, working ratio, etc, error propagation was used [36].

Table 2: Measurement parameters and associated uncertainty.

Parameter	**Unit**	x_{avg}	σ_x	$\frac{\sigma_x}{x_{avg}} \times 100\%$
Air inlet temperature	°C	27.2	±0.1	0.36%
Air outlet temperature	°C	16.6	±0.5	3.01%
Air inlet Relative Humidity	%	36.0	±0.4	1.11%
Air outlet Relative Humidity	%	71.4	±1.2	1.68%
Time	s	—	±0.01	—
Mass	g	—	±0.007	—
Dimensions	mm	—	±1.0	—
Air flow rate	kg/s	—	±0.01	—
Voltage	V	220.0	±2.4	1.09%
Current	A	2.6	±0.1	3.85%
Wet bulb efficiency (η_{WB})	%	90.9	±6.4	7.04%
Dew point efficiency (η_{DP})	%	55.9	±2.5	4.47%
Water flow rate	kg/s	0.05	±0.01	20%
Cooling capacity ($\dot{Q}_{cooling}$)	kW	10.71	±0.29	2.71%
Input power ($\dot{Q}_{input}$)	W	573.2	±38.3	6.68%
COP		56.8	±5.4	9.51%
EER		241.7	±7.7	3.18%

3. Results

3.1. Variations in airflow rate

All experiments in this section were conducted at a constant inlet dry bulb temperature of $T_{DBT} = 27.2$°C and relative humidity of 36%, corresponding to a wet bulb temperature of $T_{WBT} = 17.15$°C and a dew point temperature of $T_{DPT} = 10.87$°C. The flow rate of the air entering the dry channel was increased from a small value of 100 m^3/h to 11,000 m^3/h. The changes in different parameters like the product air temperature, cooling capacity, fan and pump power consumption, COP, and Wet-bulb and Dewpoint efficiency with respect to airflow are shown in Fig # 6.

Fig # 6 (a) shows that the lowest product air temperature is observed at the smallest airflow rate, and it the temperature goes up with airflow. This is an expected finding since increasing the air flow rate allows the air less time to stay in contact with water in the wet channel, reducing the temperature drop due to evaporation [38]. As the airflow rate increases, the product air temperature approaches the ambient temperature, i.e., the temperature drop or the range ΔT_{range} diminishes. This is concurrent with other studies that suggest that very high flow rates move so much air through a heat and mass exchanger that the cooling system is unable to cause a significant temperature drop across the air [30]. It can also be observed that the temperature decreases as the working ratio r is increased, confirming that spending a higher proportion of the dry air on recirculation and mixing in the wet channel results in a larger temperature drop [18]. It must be noted that for this study, the results are based on a consistent inlet air temperature. The outlet air was not recirculated back, and the system was kept open loop to maintain constant inlet temperatures and humidity and prevent the indoor climate conditions from impacting inlet variables. Variations in inlet air temperature and humidity would cause changes in the product air temperature [44].

However, the higher temperature drop observed at high working ratios as shown in Fig # 6 (a), comes with a tradeoff. Fig # 6 (b) shows the cooling capacity of the M-cycle. Similar curves for cooling capacity have been reported in other studies [7, 45]. It can be observed that using very low flow rates to attain very low temperatures results in a very small cooling capacity. This is due to the low flow rate of the inlet air, compounded by the high working ratio, resulting in most of the cooled product air being lost for recirculation.

More importantly, it was found that the cooling capacity peaked at moderate flow rates and the highest cooling capacity was observed for a moderate working ratio of $r = 0.33$. This finding is consistent with the results obtained in other studies. Zhu et al [46] found the optimal cooling capacity for a fixed flow rate occurring at the same working ratio of $r = 0.33$. Lin et al [31] found a slightly higher optimal working air ratio at $r = 0.40$. Wang et al [29] found that when the airflow was kept constant, the cooling capacity peaked at working ratios ranging from $r = 0.29$ to $r = 0.35$. They also found that the peak cooling capacity went up with airflow rate, but their study was focused on lower flow rates ($\leq 950\ m^3/hr$). The results shown in Fig # 6 (b) demonstrate that increasing the flow rate to very high levels ($\geq 10,000\ m^3/hr$) results in a drop in cooling capacity for $r = 0.33$. This is because, as the flow rate rises, the temperature drop across the dry channel ΔT_{range} reduces since the air is unable to evaporate enough water, requiring a larger heat and mass exchanger to achieve a large enough ΔT_{range}.

Prior to this drop, a flattening of the cooling capacity and COP curves is observed at moderate flow rates. This occurs because the cooling capacity gain from increasing the mass flow rate of product air is progressively offset by the diminishing ΔT_{range}, as the residence time of air in the heat and mass exchanger becomes too short for sufficient heat and mass transfer. The two competing effects, increasing mass flow and decreasing temperature drop, balance each other out, resulting in the plateau observed before the eventual decline at very high flow rates.

Fig # 6 (c) shows that the system power consumption goes up as the airflow rate is increased. But it also shows that recirculating more air into the wet channel increases the power consumption of the overall system compared to lower working ratios. This finding is in contrast to some studies which have found the dry channel's fan power to go down with working ratio [29]. But it is in agreement with other studies which have found the pressure drop, and thereby the power consumption to increase with the working air ratio [47, 48]. The difference is related to the configuration and the operational equipment. In counterflow configurations, air in dry channels has to change directions to enter the wet channel as illustrated in Fig # 3 (b). This results in a high pressure drop which for the fan to overcome [29]. In the design used in this study, the recirculating product air had to undergo two 90^o bends to enter the wet channel, resulting in a high pressure drop for the fan to overcome, resulting in an increase in fan power with the working air ratio.

As a result of the increasing power consumption with the working air ratio, the COP is found to decrease with the working air ratio as shown in Fig # 6 (d). However, due to the cooling capacity rising until a maximum at moderate flow rates, the COP for each working air ratio follows the same trend. It must be noted that the high COP observed for very low working ratios is only an artifact of the high flow rate of the product air, since very little dry channel air is used for recirculation and exhausted [49]. But this improvement comes at the cost of an overall higher product air temperature as shown in Fig # 6 (a).

Both wet-bulb and dew point efficiencies go down with airflow rate and increase with the working air ratio. This is a typical and expected result that matches with other studies in the literature [31]. The temperature drop efficiency reduces with flow rate because the heat and mass exchanger is not large enough to allow 13000 m^3/hr of air to undergo a large enough temperature drop. And the efficiency improves with the working air ratio because recirculating a large proportion of dry air to turn it into working air results in more evaporation of water in the wet channel and therefore larger temperature drops [29].

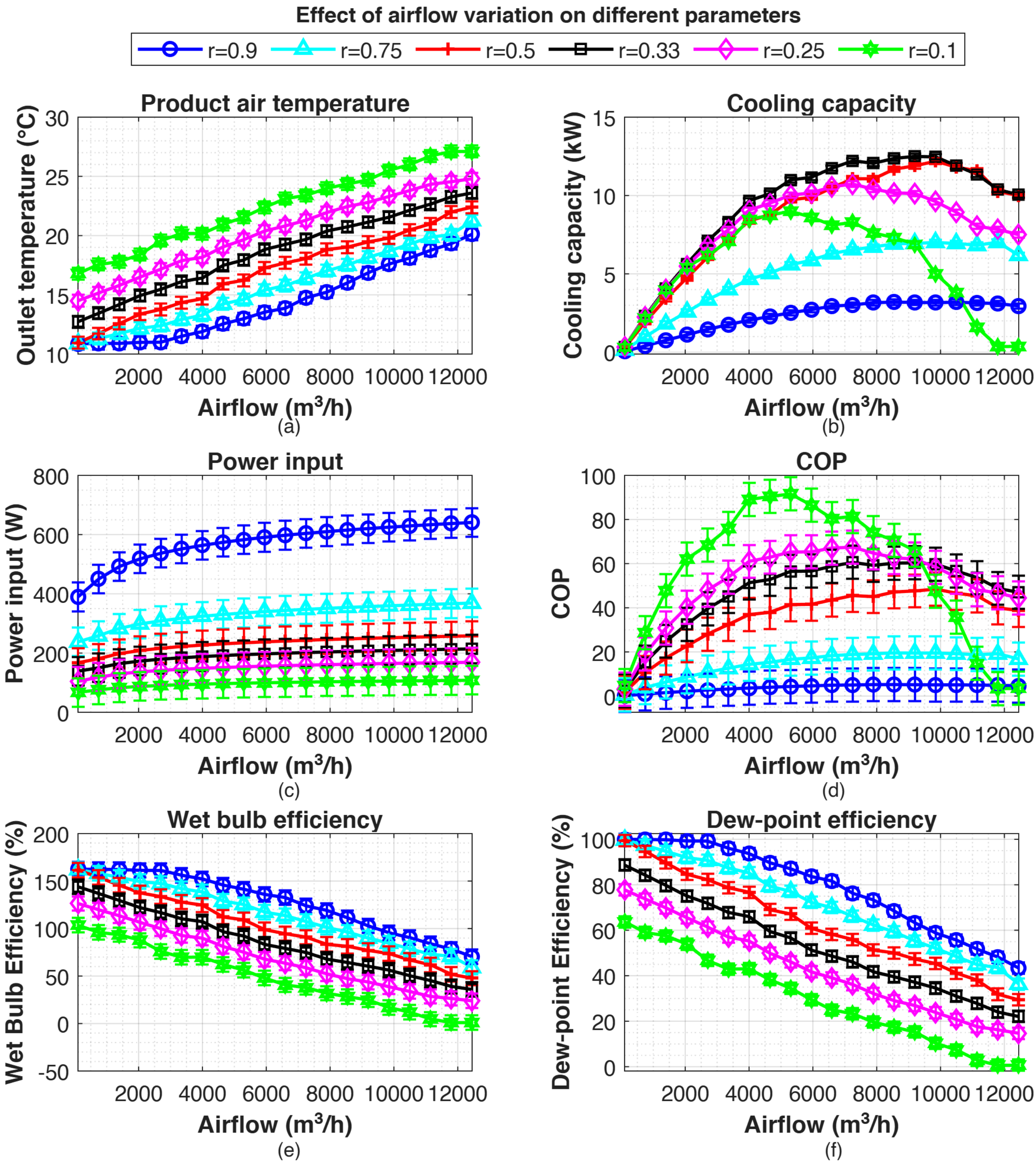

Figure 6: Variation of (a) Product air temperature, (b) Cooling capacity, (c) Power input, (d) COP, (e) Wet bulb efficiency, and (f) Dew-point efficiency vs airflow rate at inlet conditions of $T_{DBT} = 27.2$°C and RH $= 36\%$, for working air distribution ratio $r_d = 1.0$ and varying working air ratios r. Product air temperature increases with airflow while cooling capacity peaks at moderate flow rates, with $r = 0.33$ yielding the optimal balance between cooling capacity and COP. Erorr bars are based on two (2) standard deviations $\pm 2\sigma$.

3.2. Changes in where the product air is taken out for recirculation

As with Section 3.1, all experiments were conducted at a constant inlet dry bulb temperature of $T_{DBT} = 27.2$°C and relative humidity of 36% at a fixed airflow rate of 6600 m^3/hr. Fig # 7 shows the variation in temperature, cooling capacity, power input, COP, and wet bulb and dew point efficiencies as the working air distribution ratio r_d is varied, i.e., whether the dry air used to enter the wet channel comes from upstream or downstream of the dry channel. All of the results are recorded at a fixed airflow rate of 6600 m^3/hr.

Fig # 7 (a) shows that until a minimum temperature, as r_d increases, the temperature of the product air goes down, suggesting that drawing air from downstream of the dry channel leads to a larger temperature drop regardless of the overall working air ratio r. There is no study in the literature testing the impact of upstream vs downstream draw of dry air but several findings in literature suggest that the temperature drop achieved with each cycle or stage of recirculation reduces [46], a finding that is also consistent with psychrometry as illustrated in Fig # 2 where $\Delta T_1 > \Delta T_2 > \Delta T_3$.

It must be noted that the temperature reaches a minimum at r_d values slightly larger than one after which it starts increasing back up. The reason for that is that as r_d approaches very small values close to zero, the system starts resembling a single-stage dew-point cooler with air being drawn halfway through the dry channel as illustrated in Fig # 5 (a) ($r_d = 0$). The system resembles a typical 2-stage dew-point cooler when the airflow through both the upstream and downstream valves is comparable as shown in Fig # 5 (c) ($r_d = 1$). But as r_d approaches very large values well beyond 1.0, the system starts operating like a single-stage dew-point cooler again but with the air being drawn primarily downstream of the dry channel as illustrated in Fig # 5 (h) ($r_d = \infty$). The wet-bulb and dew-point efficiencies shown in Fig # 7 (e) and Fig # 7 (f) follow the inverted trend of the temperature curve as the effectiveness of the cooling improves as temperature goes down.

The finding that the minimum temperature was observed at $r_d \approx 1.5$ suggests that there is an advantage to drawing more dry air downstream of the dry channel. This is because the dry air is much cooler downstream of the flow and thereby results in a larger temperature drop when it is recirculated to act as the process air. As shown in Fig # 7 (b), It follows from the lower temperatures observed at $rd \approx 1.5$ that the cooling capacity is also at its maximum at this point, given that the overall mass flow rate of the air is unchanged for each overall working air ratio r. However, the power consumption does not just depend on the working air ratio and airflow. As shown in Fig # 7 (c), the fan power consumption increases with r_d. This is because a larger pressure drop is needed across the dry channel if more air is to be taken fully downstream to be recirculated.

But the more critical finding represented in Fig # 7 (a) and Fig # 7 (d) is that drawing an excessive volume of air downstream of the dry channel with a minimal proportion of recirculated air coming from upstream results in a lower temperature drop while the power consumption keeps going up due to increasing pressure drop. Based on the minimum temperature and the maximum COP observed at $1.1 \leq r_d \leq 1.3$, it can be said that the volume flow rate of air drawn in each stage of a dew-point cooler should be almost equal, resulting in $r_d = 1$. Due to pressure losses in the wet and dry channels, this optimal distribution ratio is not ensured, and it can be made part of the design process. For perforated dew-point coolers, this means that not all perforations have to be equally sized. The perforations can be sized such that there is a similar air flow through each perforation, accounting for the pressure drops.

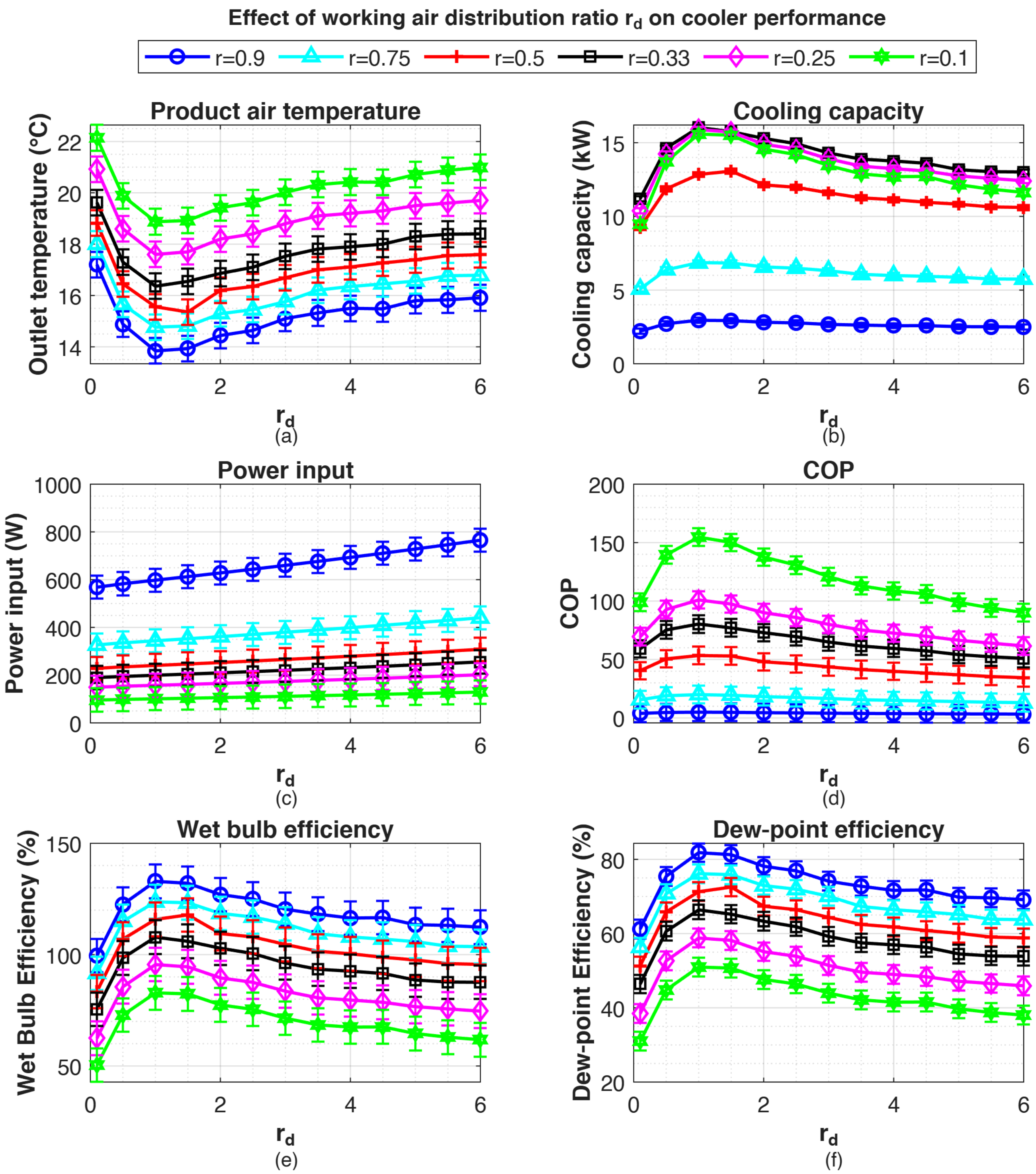

Figure 7: Variation of (a) Product air temperature, (b) Cooling capacity, (c) Power input, (d) COP, (e) Wet bulb efficiency, and (f) Dew-point efficiency vs working air distribution ratio $r_d = \dot{V}_2/\dot{V}_1$, representing the ratio of air drawn from downstream to upstream of the dry channel, at $T_{DBT} = 27.2$°C, RH $= 36\%$, and airflow rate of 6600 m^3/hr, for varying working air ratios r. A minimum product air temperature and maximum COP are observed at $1.1 \leq r_d \leq 1.3$, suggesting an advantage to drawing slightly more air from downstream of the dry channel. Erorr bars are based on two (2) standard deviations $\pm 2\sigma$.

3.3. Impact of RH

The inlet dry bulb temperature was maintained at $T_{DBT} = 27.2$°C throughout, while the relative humidity was varied across a wide range while maintaining the air temperature T_i with an extra water evaporator and a resistive heater, the input power of which was PID-controlled. As shown in Figure 8 (a), it was found that the product air temperature approaches the dry bulb temperature with increase in RH. The temperature drop curve matches that for similar studies in literature [50, 51]. At high humidity levels, there is negligible or no temperature drop in the product air. But the power consumption of the system remains unchanged and is independent of the humidity of the incoming air. Due to the low temperature drop at high humidity without any difference in power use, the cooling capacity and COP of the system drastically reduce as shown in Figures 8 (b), (c), and (d). Cooling capacity and cOP approach zero as the temperature drive is eliminated. This is a very typical and expected finding for all evaporative systems since the amount of water air can evaporate is heavily governed by the humidity of air feed [52].

As shown in Figures 8 (c) and (d), the Wet Bulb and Dew Point Efficiencies start at very high levels because low humidity levels drastically drop the Wet Bulb and Dew Point temperatures, and therefore the temperature drop observed across the dry channel. It must be noted that in ambient conditions, Dew-Point effectiveness can never exceed 100%. It is higher than 100% in Figure 8 (d) below ambient humidity levels because the inlet air's humidity was artificially dropped, reducing the DPT of the product air while keeping the ambient DPT the same. The effectiveness curves closely resemble the observations found by Wan et al [53] for an experimentally validated model.

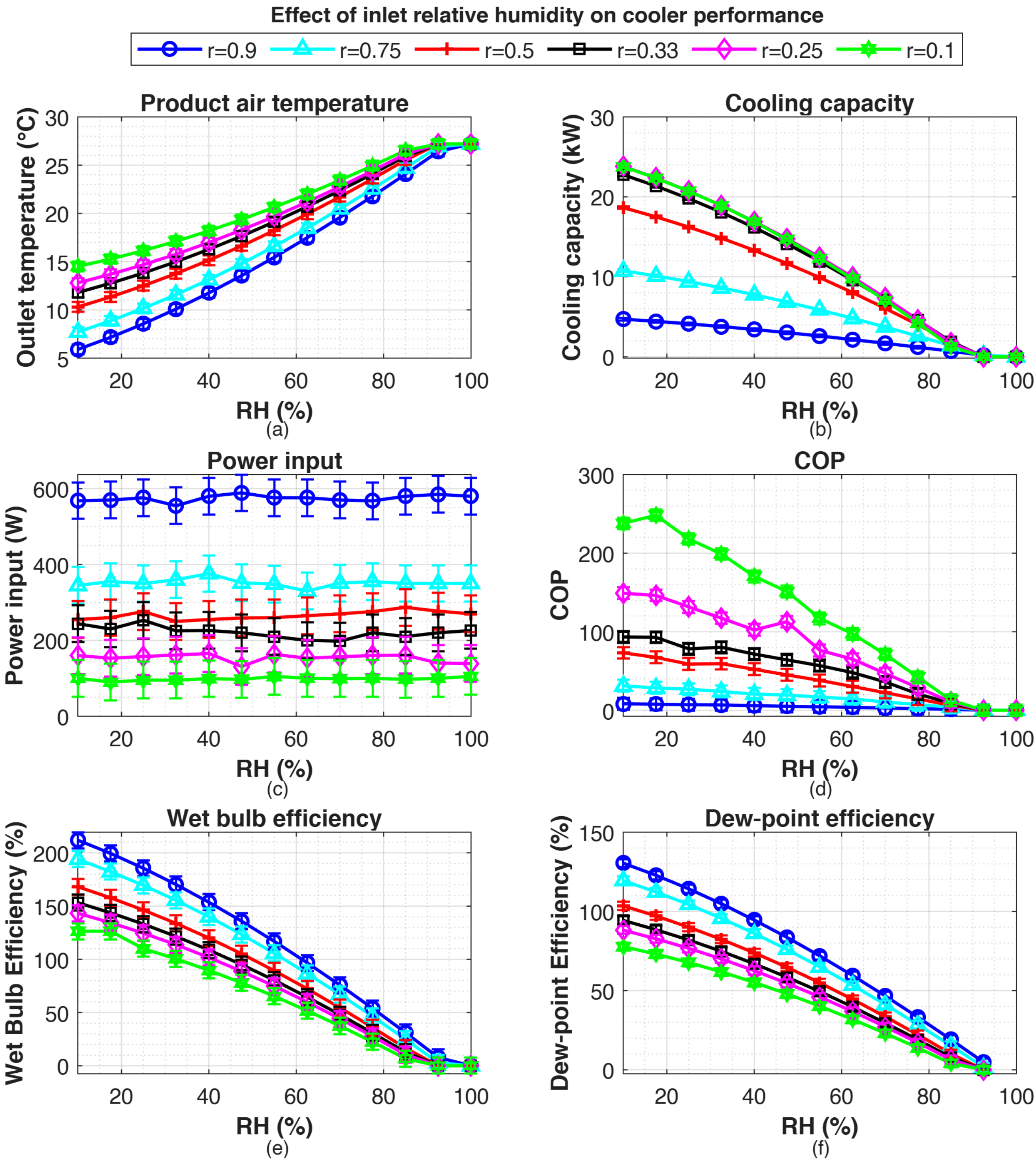

Figure 8: Variation of (a) Product air temperature, (b) Cooling capacity, (c) Power input, (d) COP, (e) Wet bulb efficiency, and (f) Dew-point efficiency vs inlet relative humidity at $T_{DBT} = 27.2$°C, for working air distribution ratio $r_d = 1.0$ and varying working air ratios r. Cooling capacity and COP diminish sharply with increasing humidity, approaching zero at high RH levels, while dew-point effectiveness exceeds 100% at artificially reduced humidity levels because T_{DPT} is reduced below ambient conditions. Erorr bars are based on two (2) standard deviations $\pm 2\sigma$.

4. Conclusion

The study explores the performance of a large-scale dew point cooler with a cooling capacity of 12.2 kW. Two controllable recirculation stages were incorporated to benchmark the working air ratio r against other studies. A new parameter, the air distribution ratio r_d, was evaluated based on the amount of air drawn in each recirculation stage.

The results confirm that increasing the working air ratio improves temperature drop and dew-point effectiveness but reduces COP due to higher power consumption from increased pressure losses incurred during recirculation. Low working air ratio was found to result in small temperature drops, and very high working air ratios were found to result in large temperature drops, yielding high Dew-point efficiencies at the cost of losing the product air volume. An optimal working air ratio of $r = 0.33$ was identified for maximizing the COP and the cooling capacity. This finding is consistent with the optimum working air ratios reported in the literature.

The investigation of the working air distribution ratio r_d is a novel contribution of this work. It was found that drawing recirculated air preferentially from downstream of the dry channel, where the product air is already partially cooled, reduces the product air temperature without the need to increase the overall working air ratio or cut down on the product air volume. Since the power consumption has a very small correlation with the air distribution ratio, the overall COP goes up at the optimal distribution ratio of $1.1 \leq r_d \leq 1.3$. This finding suggests that for M-cycle heat exchangers, perforation sizing or duct sizing should account for channel pressure drops to maintain near-equal airflow through each recirculation stage.

This study is based on only two recirculation cycles. Further computational and experimental studies can test if the optimal air distribution holds up for more recirculation loops or a large number of perforations. Further studies could also assess the pressure drop across each circulation loop and mitigate it with surface treatments or smoother bends. That would in turn help maintain optimal air distribution ratios and thereby maximize the COP and cooling capacity without compromising on the product air temperature.

To illustrate the practical utility of these findings, consider a representative operating condition of inlet air at 35°C and 40% RH, typical of hot and arid climates where dew-point coolers are most effective. Based on the experimental results, the recommended operating settings for this condition are a working air ratio of $r = 0.33$ and a working air distribution ratio of $1.1 \leq r_d \leq 1.3$, with an airflow rate in the moderate range of 6000-7000 m^3/hr where cooling capacity peaks. Under these settings, the system is expected to deliver the lowest achievable product air temperature while maintaining the highest COP, making it suitable for direct space cooling without supplementary mechanical refrigeration. It should be noted, however, that performance degrades significantly above ∼60% RH, and inlet air pre-treatment is recommended for deployment in humid climates. This serves as a practical design guideline for engineers deploying large-scale M-cycle dew-point coolers in similar climatic conditions.

References

[1] F. Pavanello, E. De Cian, M. Davide, M. Mistry, T. Cruz, P. Bezerra, D. Jagu, S. Renner, R. Schaeffer, A. F. P. Lucena, Air-conditioning and the adaptation cooling deficit in emerging economies, Nature Communications 12 (1) (2021) 6460. doi:10.1038/s41467-021-26592-2.
URL https://doi.org/10.1038/s41467-021-26592-2

[2] E. Elnagar, A. Arteconi, P. Heiselberg, V. Lemort, Integration of resilient cooling technologies in building stock: Impact on thermal comfort, final energy consumption, and ghg emissions, Building and Environment 261 (2024) 111666. doi:https://doi.org/10.1016/j.buildenv.2024.111666.
URL https://www.sciencedirect.com/science/article/pii/S0360132324005080

[3] P. Sherman, H. Lin, M. McElroy, Projected global demand for air conditioning associated with extreme heat and implications for electricity grids in poorer countries, Energy and Buildings 268 (2022) 112198. doi:https://doi.org/10.1016/j.enbuild.2022.112198.
URL https://www.sciencedirect.com/science/article/pii/S0378778822003693

[4] Z. Sun, Q. Wang, Y. Yuan, D. Wang, Q. Zhou, C. Xu, K. Meng, H. Peng, L. Yan, R. Jin, L. Li, H. Liu, Y. Wang, J. Hu, Experimental analysis of a co2 closed heat pump drying system combined with rotary dehumidification for drying banana slices drying, International Journal of Refrigeration 160 (2024) 76–87. doi:https://doi.org/10.1016/j.ijrefrig.2024.01.017.
URL https://www.sciencedirect.com/science/article/pii/S0140700724000264

[5] H. A. Al Khiro, R. Boukhanouf, Analytical and computer modelling of a thermo-mechanical vapour compression system for space air conditioning in buildings, Energy Conversion and Management 323 (2025) 119252. doi:https://doi.org/10.1016/j.enconman.2024.119252.
URL https://www.sciencedirect.com/science/article/pii/S0196890424011932

[6] B. Hu, H. Liu, J. Jiang, Z. Zhang, H. Li, R. Wang, Ten megawatt scale vapor compression heat pump for low temperature waste heat recovery: Onsite application research, Energy 238 (2022) 121699. doi:https://doi.org/10.1016/j.energy.2021.121699.
URL https://www.sciencedirect.com/science/article/pii/S0360544221019472

[7] Y. Yang, B. Yang, J. Zeng, L. Yin, Z. Xie, Exergy analysis of hybrid air-conditioning systems with different evaporative-cooling condensers under hot-humid climates, Journal of Building Engineering 97 (2024) 110692. doi:https://doi.org/10.1016/j.jobe.2024.110692.
URL https://www.sciencedirect.com/science/article/pii/S2352710224022605

[8] A. Wu, Z. Hao, D. Cai, X. Wang, G. He, Thermodynamic, environmental, and economic analysis of a novel dual-mode ejector-enhanced co2 cooling and heating system, Energy 340 (2025) 139355. doi:https://doi.org/10.1016/j.energy.2025.139355.
URL https://www.sciencedirect.com/science/article/pii/S0360544225049977

[9] S. Abdullah, M. N. B. M. Zubir, M. R. B. Muhamad, K. M. S. Newaz, H. F. Öztop, M. S. Alam, K. Shaikh, Technological development of evaporative cooling systems and its integration with air dehumidification processes: A review, Energy and Buildings 283 (2023) 112805. doi:https://doi.org/10.1016/j.enbuild.2023.112805.
URL https://www.sciencedirect.com/science/article/pii/S037877882300035X

[10] A. M. Zaki, M. H. Bargal, M. A. Antar, E. M. Mokheimer, L. M. Alhems, Advances in indirect evaporative cooling: principles, integrated cycles, economic insights, and environmental implications, Thermal Science and Engineering Progress 67 (2025) 104078. doi:https://doi.org/10.1016/j.tsep.2025.104078.
URL https://www.sciencedirect.com/science/article/pii/S2451904925008698

[11] A. Adam, D. Han, W. He, M. Amidpour, Analysis of indirect evaporative cooler performance under various heat and mass exchanger dimensions and flow parameters, International Journal of Heat and Mass Transfer 176 (2021) 121299. doi:https://doi.org/10.1016/j.ijheatmasstransfer.2021.121299.
URL https://www.sciencedirect.com/science/article/pii/S0017931021004026

[12] Z. Chen, W. Zhao, B. Wang, L. Huang, J. Ding, G. Cheng, D. Bui, A first-of-its-kind two-stage dew-point evaporative cooler with high energy efficiency and compact design, Energy Conversion and Management 341 (2025) 120090. doi:https://doi.org/10.1016/j.enconman.2025.120090.
URL https://www.sciencedirect.com/science/article/pii/S0196890425006144

[13] A. HS, M. N, S. Shenoy, S. Kumar, Performance evaluation of an indirect-direct evaporative cooler using biomass-based packing material, International Journal of Sustainable Engineering 17 (1) (2024) 469–480. arXiv:https://doi.org/10.1080/19397038.2024.2360451, doi:10.1080/19397038.2024.2360451.
URL https://doi.org/10.1080/19397038.2024.2360451

[14] The Maisotsenko Cycle for Electronics Cooling, Vol. Advances in Electronic Packaging, Parts A, B, and C of International Electronic Packaging Technical Conference and Exhibition. arXiv:https://asmedigitalcollection.asme.org/InterPACK/proceedings-pdf/InterPACK2005/42002/415/4531565/415_1.pdf, doi:10.1115/IPACK2005-73283.
URL https://doi.org/10.1115/IPACK2005-73283

[15] B. A. Salman, Performance analysis of a conventional two-stage indirect evaporative cooler, International Journal of Air-Conditioning and Refrigeration 32 (1) (2024) 18. doi:10.1007/s44189-024-00063-x.
URL https://doi.org/10.1007/s44189-024-00063-x

[16] K. Wu, S. Wang, J. Lin, Y. Shao, F. Gao, K. J. Chua, The enhanced dew-point evaporative cooling with a macro-roughened structure, International Journal of Heat and Mass Transfer 219 (2024) 124898. doi:https://doi.org/10.1016/j.ijheatmasstransfer.2023.124898.
URL https://www.sciencedirect.com/science/article/pii/S0017931023010438

[17] Z. Chen, B. Wang, L. Huang, Z. Yang, G. Cheng, D. Bui, Energy-efficient cooling beyond m–cycle: development and evaluation of a two-stage dew-point evaporative cooler, Applied Thermal Engineering 280 (2025) 128031. doi:https://doi.org/10.1016/j.applthermaleng.2025.128031.
URL https://www.sciencedirect.com/science/article/pii/S1359431125026237

[18] P. Xu, X. Mu, H. Chen, X. Ma, X. Zhao, Experimental and numerical investigation of the temperature and humidity distribution inside the channels for a regenerative indirect evaporative cooler, Applied Thermal Engineering 236 (2024) 121586. doi:https://doi.org/10.1016/j.applthermaleng.2023.121586.
URL https://www.sciencedirect.com/science/article/pii/S1359431123016150

[19] G. Zhu, T. Wen, Q. Wang, X. Xu, A review of dew-point evaporative cooling: Recent advances and future development, Applied Energy 312 (2022) 118785. doi:https://doi.org/10.1016/j.apenergy.2022.118785.
URL https://www.sciencedirect.com/science/article/pii/S0306261922002343

[20] Z. Duan, X. Zhao, C. Zhan, X. Dong, H. Chen, Energy saving potential of a counter-flow regenerative evaporative cooler for various climates of china: Experiment-based evaluation, Energy and Buildings 148 (2017) 199–210. doi:https://doi.org/10.1016/j.enbuild.2017.04.012.
URL https://www.sciencedirect.com/science/article/pii/S0378778816315560

[21] X. Ma, C. Zeng, Z. Zhu, X. Zhao, X. Xiao, Y. G. Akhlaghi, S. Shittu, Real life test of a novel super performance dew point cooling system in operational live data centre, Applied Energy 348 (2023) 121483. doi:https://doi.org/10.1016/j.apenergy.2023.121483.
URL https://www.sciencedirect.com/science/article/pii/S0306261923008474

[22] M. Jradi, S. Riffat, Experimental and numerical investigation of a dew-point cooling system for thermal comfort in buildings, Applied Energy 132 (2014) 524–535. doi:https://doi.org/10.1016/j.apenergy.2014.07.040.
URL https://www.sciencedirect.com/science/article/pii/S0306261914007223

[23] D. M. Weragoda, G. Tian, Q. Cai, T. Zhang, K. H. Lo, Numerical investigation of the saturation effect on wick dry-out in a capillary driven evaporative cooling system, International Communications in Heat and Mass Transfer 155 (2024) 107490. doi:https://doi.org/10.1016/j.icheatmasstransfer.2024.107490.
URL https://www.sciencedirect.com/science/article/pii/S0735193324002525

[24] B. Wang, M. Garcia, C. Wei, G. Cheng, W. Pang, T. Bui, Development and performance analysis of a compact counterflow dew-point cooler for tropics, Thermal Science and Engineering Progress 46 (2023) 102218. doi:https://doi.org/10.1016/j.tsep.2023.102218.
URL https://www.sciencedirect.com/science/article/pii/S2451904923005711

[25] Y. Liu, Y. G. Akhlaghi, X. Zhao, J. Li, Experimental and numerical investigation of a high-efficiency dew-point evaporative cooler, Energy and Buildings 197 (2019) 120–130. doi:https://doi.org/10.1016/j.enbuild.2019.05.038.
URL https://www.sciencedirect.com/science/article/pii/S0378778819304694

[26] O. Khalid, M. Ali, N. A. Sheikh, H. M. Ali, M. Shehryar, Experimental analysis of an improved maisotsenko cycle design under low velocity conditions, Applied Thermal Engineering 95 (2016) 288–295. doi:https://doi.org/10.1016/j.applthermaleng.2015.11.030.
URL https://www.sciencedirect.com/science/article/pii/S1359431115012661

[27] S. Huang, W. Li, J. Lu, Y. Li, Experimental study on two type of indirect evaporative cooling heat recovery ventilator, Procedia Engineering 205 (2017) 4105–4110, 10th International Symposium

on Heating, Ventilation and Air Conditioning, ISHVAC2017, 19-22 October 2017, Jinan, China. doi:https://doi.org/10.1016/j.proeng.2017.09.910.
URL https://www.sciencedirect.com/science/article/pii/S1877705817344685

[28] P. Xu, X. Ma, X. Zhao, K. Fancey, Experimental investigation of a super performance dew point air cooler, Applied Energy 203 (2017) 761–777. doi:https://doi.org/10.1016/j.apenergy.2017.06.095.
URL https://www.sciencedirect.com/science/article/pii/S0306261917308528

[29] B. Wang, Z. Chen, G. You, J. Ding, G. Cheng, T. Bui, Performance assessment of a high-efficiency indirect dew-point evaporative cooler through three-dimensional modeling, Energy 312 (2024) 133422. doi:https://doi.org/10.1016/j.energy.2024.133422.
URL https://www.sciencedirect.com/science/article/pii/S0360544224031980

[30] X. Liu, C. Jing, Y. Li, S. Lu, Study on performance of perforated dew point indirect evaporative coolers, Scientific Reports 15 (1) (2025) 939. doi:10.1038/s41598-025-85253-2.
URL https://doi.org/10.1038/s41598-025-85253-2

[31] J. Lin, R. Wang, C. Li, S. Wang, J. Long, K. J. Chua, Towards a thermodynamically favorable dew point evaporative cooler via optimization, Energy Conversion and Management 203 (2020) 112224. doi:https://doi.org/10.1016/j.enconman.2019.112224.
URL https://www.sciencedirect.com/science/article/pii/S0196890419312300

[32] A. Urso, E. Velasco-Gómez, A. Tejero-González, M. Andrés-Chicote, F. Nocera, Experimental study of the optimal design and performance of a mixed-flow dew-point indirect evaporative cooler, Applied Thermal Engineering 257 (2024) 124294. doi:https://doi.org/10.1016/j.applthermaleng.2024.124294.
URL https://www.sciencedirect.com/science/article/pii/S1359431124019628

[33] Y. You, G. Wang, B. Yang, C. Guo, Y. Ma, B. Cheng, Study on heat transfer characteristics of indirect evaporative cooling system based on secondary side hydrophilic, Energy and Buildings 257 (2022) 111704. doi:https://doi.org/10.1016/j.enbuild.2021.111704.
URL https://www.sciencedirect.com/science/article/pii/S0378778821009889

[34] X. LIU, C. JING, Y. ZHAO, T. MIYAZAKI, Numerical study on performance of the dew point evaporative cooling system, Journal of Thermal Science and Technology 16 (3) (2021) JTST0040–JTST0040. doi:10.1299/jtst.2021jtst0040.

[35] M. Hamalian, A. Bhati, K. Maynor, V. Bahadur, Techno-economic analysis of electrochemical carbon capture from oceanwater integrated with hydrates-based sequestration, Applied Energy 392 (2025) 125960. doi:https://doi.org/10.1016/j.apenergy.2025.125960.
URL https://www.sciencedirect.com/science/article/pii/S0306261925006907

[36] M. Usama, Z. Ali, M. C. Ndukwu, R. Sathyamurthy, The energy, emissions, and drying kinetics of three-stage solar, microwave and desiccant absorption drying of potato slices, Renewable Energy 219 (2023) 119509. doi:https://doi.org/10.1016/j.renene.2023.119509.
URL https://www.sciencedirect.com/science/article/pii/S0960148123014246

[37] S. Rasheed, M. Ali, H. Ali, N. A. Sheikh, Experimental evaluation of indirect evaporative cooler with improved heat and mass transfer, Applied Thermal Engineering 217 (2022) 119152. doi:https://doi.org/10.1016/j.applthermaleng.2022.119152.
URL https://www.sciencedirect.com/science/article/pii/S1359431122010833

[38] X. Xiao, J. Liu, A state-of-art review of dew point evaporative cooling technology and integrated applications, Renewable and Sustainable Energy Reviews 191 (2024) 114142. doi:https://doi.org/10.1016/j.rser.2023.114142.
URL https://www.sciencedirect.com/science/article/pii/S1364032123010006

[39] R. Kousar, M. Ali, N. A. Sheikh, S. I. ul Haq Gilani, S. Khushnood, Holistic integration of multi-stage dew point counter flow indirect evaporative cooler with the solar-assisted desiccant cooling system: A techno-economic evaluation, Energy for Sustainable Development 62 (2021) 163–174. doi:https://doi.org/10.1016/j.esd.2021.04.005.
URL https://www.sciencedirect.com/science/article/pii/S097308262100051X

[40] D. Pandelidis, S. Anisimov, Numerical analysis of the heat and mass transfer processes in selected m-cycle heat exchangers for the dew point evaporative cooling, Energy Conversion and Management 90 (2015) 62–83. doi:https://doi.org/10.1016/j.enconman.2014.11.008.
URL https://www.sciencedirect.com/science/article/pii/S0196890414009649

[41] L. Jia, J. Liu, C. Wang, X. Cao, Z. Zhang, Study of the thermal performance of a novel dew point evaporative cooler, Applied Thermal Engineering 160 (2019) 114069. doi:https://doi.org/10.1016/j.applthermaleng.2019.114069.
URL https://www.sciencedirect.com/science/article/pii/S1359431118376919

[42] S. Bilyaz, A. Bhati, M. Hamalian, K. Maynor, T. Soori, A. Gattozzi, C. Penney, D. Weeks, Y. Xu, L. Hu, J. Zhu, J. Nelson, R. Hebner, V. Bahadur, Modeling the impact of high thermal conductivity paper on the performance and life of power transformers, Heliyon 10 (6) (2024) e27783. doi:10.1016/j.heliyon.2024.e27783.
URL https://doi.org/10.1016/j.heliyon.2024.e27783

[43] M. Usama, Z. Ali, A. Iqbal, M. C. Ndukwu, Controlling surface temperature in intermittent microwave drying of potato slices using evaporative cooling: An experimental study, Innovative Food Science Emerging Technologies 109 (2026) 104470. doi:https://doi.org/10.1016/j.ifset.2026.104470.
URL https://www.sciencedirect.com/science/article/pii/S146685642600038X

[44] I. Khan, W. Khalid, H. M. Ali, S. M. Hasan, Z. Atif, E. Uddin, Numerical and experimental investigation of a novel hybrid indirect-direct evaporative cooling system with enhanced humidity regulation: A case study in hot-humid conditions, Case Studies in Thermal Engineering 77 (2026) 107538. doi:https://doi.org/10.1016/j.csite.2025.107538. URL https://www.sciencedirect.com/science/article/pii/S2214157X25017988

[45] S. Rasheed, M. Ali, H. Ali, N. A. Sheikh, G. Li, Design evolution of indirect evaporative air-cooling system through multiple configurations for the enhancement of heat and mass transfer mechanism, International Communications in Heat and Mass Transfer 160 (2025) 108393. doi:https://doi.org/10.1016/j.icheatmasstransfer.2024.108393. URL https://www.sciencedirect.com/science/article/pii/S0735193324011552

[46] G. Zhu, W. Chen, D. Zhang, T. Wen, Performance evaluation of counter flow dew-point evaporative cooler with a three-dimensional numerical model, Applied Thermal Engineering 219 (2023) 119483. doi:https://doi.org/10.1016/j.applthermaleng.2022.119483. URL https://www.sciencedirect.com/science/article/pii/S1359431122014132

[47] J. Lin, D. T. Bui, R. Wang, K. J. Chua, On the exergy analysis of the counter-flow dew point evaporative cooler, Energy 165 (2018) 958–971. doi:https://doi.org/10.1016/j.energy.2018.10.042. URL https://www.sciencedirect.com/science/article/pii/S0360544218320309

[48] J. Lin, D. T. Bui, R. Wang, K. J. Chua, The counter-flow dew point evaporative cooler: Analyzing its transient and steady-state behavior, Applied Thermal Engineering 143 (2018) 34–47. doi:https://doi.org/10.1016/j.applthermaleng.2018.07.092. URL https://www.sciencedirect.com/science/article/pii/S1359431118309025

[49] S. Rasheed, M. Ali, H. Ali, N. A. Sheikh, M. Imran, X. Xie, G. Li, Enhanced thermal efficiency in crossflow evaporative cooling systems: A comparative study of materials and flow patterns, International Communications in Heat and Mass Transfer 167 (2025) 109252. doi:https://doi.org/10.1016/j.icheatmasstransfer.2025.109252. URL https://www.sciencedirect.com/science/article/pii/S0735193325006785

[50] H. M. U. Raza, M. Sultan, M. Aleem, M. W. Shahzad, M. A. Jamil, T. Miyazaki, U. Sajjad, M. Farooq, Z. Zhang, Experimental study on advanced indirect evaporative cooling and desiccant dehumidification systems for agricultural greenhouses, International Communications in Heat and Mass Transfer 172 (2026) 110321. doi:https://doi.org/10.1016/j.icheatmasstransfer.2025.110321. URL https://www.sciencedirect.com/science/article/pii/S0735193325017476

[51] F. Aldawi, Development and testing of a portable on-desk-size maisotsenko indirect evaporative cooler for central saudi arabia's climate, International Communications in Heat and Mass Transfer 169 (2025) 109820. doi:https://doi.org/10.1016/j.icheatmasstransfer.2025.109820.

URL https://www.sciencedirect.com/science/article/pii/S0735193325012461

[52] B. Wang, Z. Chen, G. You, J. Ding, G. Cheng, T. Bui, Improving indoor air quality and cooling efficiency: Indirect dew-point evaporative cooling in south china summers, Energy and Buildings 324 (2024) 114908. doi:https://doi.org/10.1016/j.enbuild.2024.114908. URL https://www.sciencedirect.com/science/article/pii/S0378778824010247

[53] Y. Wan, T. Xue, Z. Huang, A. Soh, H. Liu, K. J. Chua, Comparative study on performance of counter-flow dew-point indirect evaporative cooling systems via a more realistic and experimentally validated three-dimensional model, Journal of Building Engineering 82 (2024) 108408. doi:https://doi.org/10.1016/j.jobe.2023.108408. URL https://www.sciencedirect.com/science/article/pii/S2352710223025913

Author Contributions

Muhammad Usama: Methodology, Writing - original draft, experiments, and data interpretation. **Aashir Iqbal:** Equipment setup and process design. **Tahmid Hasan Rupam:** Review and writing. **Bidyut Baran Saha:**Review, edit, and supervision.

Declaration of Competing Interest

The authors declare that they have no known competing financial interests or personal relationships that could have appeared to influence the work reported in this paper.

Data Availability

Data will be made available on request.